CARBON 48 (2010) 3778–3787

available at www.sciencedirect.com

ScienceDirect

journal homepage: www.elsevier.com/locate/carbon

Sustainable nitrogen-doped carbonaceous materials from biomass derivatives

Li Zhao [a,b,e], *Niki Baccile* [c], *Silvia Gross* [d], *Yuanjian Zhang* [a], *Wei Wei* [b], *Yuhan Sun* [b], *Markus Antonietti* [a], *Maria-Magdalena Titirici* [a,*]

[a] *Max-Planck Institute for Colloids and Interfaces, Am Mühlenberg 1, 14424 Potsdam, Germany*
[b] *Institute of Coal Chemistry, Chinese Academy of Sciences, 030001 Taiyuan, China*
[c] *Laboratoire de Chimie de la Matière Condensée de Paris, CNRS Collège de France, 11 Place Marcelin Berthelot, 75005 Paris, France*
[d] *ISTM-CNR, Dipartimento di Scienze Chimiche and INSTM, University of Padova, Via Marzolo 1, 35131 Padova, Italy*
[e] *Graduate University of the Chinese Academy of Sciences, 100039 Beijing, China*

ARTICLE INFO

Article history:
Received 26 February 2010
Accepted 15 June 2010
Available online 22 June 2010

ABSTRACT

Nitrogen-doped carbons were produced using hydrothermal carbonization of nitrogen-containing carbohydrates under mild temperature (180 °C). The resulting materials contain significant amounts of nitrogen and display a high degree of aromatization. The nitrogen contents are also retained after further calcination at higher temperatures. All the resulting materials have been thoroughly characterized using X-ray photoelectron spectroscopy, solid state ^{15}N and ^{13}C-nuclear magnetic resonance, elemental chemical analysis, nitrogen adsorption, scanning and transmission electron microscopy. The nitrogen-doped materials proved to have superior performance with respect to their nitrogen-free counterparts in terms of electrical conductivity.

1. Introduction

Carbon materials have found a large number of applications in different domains ranging from environmental science [1,2], to drug delivery [3,4] and energy storage [5], according to their structural, morphological and chemical properties [6]. Nevertheless, for some specific applications, functionalization [7–9] is required.

The properties of carbon materials depend to a large extent on the raw material, surface structure and porosity, but also heteroatoms built into their structure exert large effects on physicochemical properties of carbons. Recently, nitrogen-containing carbons attracted particular interest due to their improved performance in applications such as CO_2 sequestration [10], removals of contaminants from gas and liquid phases [11], environmental protection [12], catalysts and catalysts supports [13], or in electrochemistry as supercapacitors [8], cells and batteries [14].

The methods for the production of such materials rely normally on very harsh and multistep processes, which involve high temperature production of carbon materials [15] followed by introduction of nitrogen into the structure using ammonia, amines or urea [16,17]. Nitrogen-containing carbons have been also more readily prepared using precursors like acetonitrile, pyrrole or polyacrylonitrile [18,19]. However, these precursors are less sustainable and available, as compared with carbohydrates which are biomass derivatives. The problem of sustainable synthesis of nanostructures carbon materials was recently revisited and implemented by several research teams [20–23], where hydrothermal treatment of biomass in water under relatively mild conditions and, in some cases, in presence of additives like metal salts

* *Corresponding author:* Fax: +49 (0) 331 567 9502.
E-mail address: magdalena.titirici@mpikg.mpg.de (M.-M. Titirici).
0008-6223/$ - see front matter
doi:10.1016/j.carbon.2010.06.040

yielded bulk, mesoporous, or nanostructured carbon materials [24–28]. Although this technique was already known since 1913 [29], the need of exploring cheap and sustainable ways to obtain chemicals [30] and carbons from raw materials other than crude oil or natural gas lead to a re-exploration of this field. In addition, the implementation of a low-cost pathway to recycle byproducts of farmed biomass would additionally represent a way to sequester significant amounts of CO_2 [31], and at the same time a material benefit would also be created.

Here we present a green and sustainable alternative to produce nitrogen rich carbonaceous materials which is based on the hydrothermal carbonization of biomass contained nitrogen-containing carbohydrates such as chitosan or glucosamine.

2. Experimental part

2.1. Materials and synthesis

All the chemicals are purchased from Sigma–Aldrich and used without further purification. Chitosan (medium molecular weight) and D(+)-glucosamine hydrochloride (>99.0%, HPLC) are the chosen biomass-derived nitrogen-containing carbohydrates. Nitrogen-doped carbons are synthesized as follows: 2 g carbohydrate and 18 g deionized water were mixed together, and then the mixture was sealed into a glass vial inside a PTFE inlets autoclave followed by hydrothermal treatment at 180 °C overnight. After the reaction, the autoclave was cooled down in a cold water bath, then the obtained black solid powder was filtered and washed with distilled water for several times. Finally, the materials were placed into a vacuum oven at 80 °C overnight for drying. The hydrothermal nitrogen-containing carbons were named as HC-chitosan (HC-CH) and HC-glucosamine (HC-GA). Afterwards, in order to improve the level of structural order, further high temperature treatment was performed in an oven under N_2 flow. The calcined samples are referred to HC-CH-750 and HC-GA-750 (where750 °C in the temperature for further calcination under a N_2 stream). To compare, non-nitrogen-containing carbons from D(+)-glucose were synthesized the same way as nitrogen doped carbon. These sample were denominated as HC-glucose (HC-G), and HC-G-750. Isotopic enrichment for solid state ^{15}N NMR was accomplished using 1 wt% of ^{15}N-labelled glucosamine (from CortecNet).

2.2. Characterization methods

The products were characterized by elemental analysis (EA) using a Vario El elemental analyzer. X-ray diffraction (XRD) patterns were recorded in reflection mode (CuKa radiation) on a Bruker D8 diffractometer oven the 2θ range of 2–80°. Scanning electron microscopy (SEM) images were acquired on a LEO 1550/LEO GmbH Oberkochen provided with an Everhard Thornley secondary electron and In-lens detectors. Transmission electron microscopy (TEM) was performed on a Zeiss EM 912 Instrument equipped with CCD camera and a filament of LaB6 under a 120 kV tension (Carl Zeiss, Oberkochen, Germany). Nitrogen adsorption and desorption isotherms were measured at 77 K with a Quadrachrome Adsorption Instrument. The Brunaer–Emmett–Teller (BET) and DFT methods were used for the surface area determination and pore size distribution calculation. Conductivity measurements were performed by I–V method with a Gamry Ref 600 Potentiostat/Galvanostat/ZRA.

Surface charge analysis – Zeta Potential measurements were realized on a Malvern Nano ZS instrument. Carbon powders were dispersed and stirred in 0.03 M NaCl solution at different pH values (0.03 M HCl and NaOH were used to adjust pH values) for two days at 25 °C to reach equilibrium. Due to the heterogeous nature of the samples, in order to avoid immediate pollution of the electrodes, all solutions were filtered by PTFE 5 μm disposable filters. Disposable clear zeta cells (DTS1060c) were used to determine the zeta potential. Gas chromatography (GC) was coupled to mass spectroscopy (MS) to separate and identify the main molecular species by mean of the NIST database included in the spectrometer software package. The instrument used is an Agilent Technologies (GC = 6890 N; MS = 5975) apparatus.

The composition of the powder was investigated by XPS. XPS spectra were run on a Perkin–Elmer 5600ci spectrometer using standard Al Kα radiation (1486.6 eV) working at 350 W. The working pressure was $<5\times10^{-8}$ Pa. The spectrometer was calibrated by assuming the binding energy (BE) of the $Au4f_{7/2}$ line at 83.9 eV with respect to the Fermi level. The standard deviation for the BE values was 0.15 eV. The reported BE were corrected for the charging effects, assigning, in the outer layers where contamination carbon is still present, to the C1s line of adventitious carbon the BE value of 284.6 eV [32,33]. Survey scans (187.85 pass energy, 1 eV/step, 25 ms per step) were obtained in the 0–1300 eV range. Detailed scans (58.7 eV pass energy, 0.1 eV/step, 100–150 ms per step) were recorded for the O1s, C1s, N1s regions. The atomic composition, after a Shirley type background subtraction [34] was evaluated using sensivity factors supplied by Perkin–Elmer [33]. Samples were introduced directly, by a fast entry lock system, into the XPS analytical chamber. The assignments of the peaks was carried out by using the values reported in the [33], in the NIST XPS Database [35] and in the references reported in the text.

^{13}C and ^{15}N solid-state MAS NMR experiments have been acquired on a Bruker Avance III 300 MHz (7.0 T), 400 MHz (9.4 T), 500 MHz (11.7 T) and 700 MHz (16.4 T) spectrometers. All ^{13}C spectra have been acquired on the 7.0 T and 9.4 T spectrometers with a 4 mm zirconia rotor as sample holder spinning at MAS rate ν_{MAS} = 14 kHz. The chemical shift reference for ^{13}C was tetramethylsilane (TMS; δ = 0 ppm) while the reported ^{15}N chemical shifts are referenced to labeled glycine at −348 ppm on the nitromethane scale (CH_3NO_2 at zero ppm).

^{13}C spectra were all recorded under cross-polarization (CP) conditions (cross polarization time is 3 s), recycle delay is 3 s and TPPM decoupling scheme is applied during signal acquisition. Number of transient is 1200 (HC-CH, HC-CH-T, HC-GA,), 2400 (HC-GA-T), 65 (pure GA), 64 (pure CH). Proton nutation (90°) frequencies were 5.40 μs and 2.32 μs, respectively, on the 9.4 T and 7.0 T spectrometers.

One pulse ^{15}N spectrum was acquired on the 11.7 T spectrometer with a 7 mm rotor (ν_{MAS} = 5 kHz) and an antiring

pulse programme (ARING) with a 90° pulse angle. ^{15}N nutation frequencies are 9.50 μs (90°) and 4.25 μs (45°) with respective recycle delays of 30 and 60 s. Number of transients is 9339 (recycle delay = 30 s) and 15,000 (recycle delay = 60 s). ^{15}N CP-MAS was performed on the 16.4 T spectrometer with a 3.2 mm rotor (ν_{MAS} = 22 kHz), 3.47 μs 90° proton pulse, number of transient is 50,971, recycle delay is 3 s and spinal-64 decoupling pulse scheme is applied during signal acquisition.

3. Results and discussion

3.1. Morphology and composition

Hydrothermal carbonization of glucose and other carbohydrates has been previously described [21], leading to carbonaceous materials [22] with applications in fields such as catalysis [36], electrochemistry [37] or adsorption [38]. This approach is extended here to the production of nitrogen doped carbon materials with chitosan (sample code HC-CH) or glucosamine (sample code HC-GA) as starting products. As-synthesized and further calcined (T = 750 °C) nitrogen containing samples were compared with the nitrogen-free ones (HC-G), as discussed in the following.

Fig. 1 shows the morphology of some hydrothermally carbonized samples. It is observed that the morphology of nitrogen containing samples is very different from the reference case of pure glucose, where hard spherical particles of ~400–500 nm diameter (SEM, Fig 1c) without inner texture (TEM, Fig 1f) are obtained [25]. In the case of chitosan no spherical particles, but a continuous network of small intercalated spheres are found, displaying a monolithic structure with an interstitial macroporosity. This can be also observed from the TEM picture in Fig. 1d which shows some intercalated, irregularly shaped spheres with a diameter of about 50 nm. Similarly, upon hydrothermal carbonization of glucosamine (Fig 1b), a compact network formed of agglomerated smaller particles has been obtained. This is clearer when looking at the TEM micrographs (Fig 1e) which reveal again such morphology with interstitial porosity. The morphology of the samples does not change after further heat treatment. Some electron micrographs of the samples treated at higher temperatures are shown in Fig. S2 – supporting information, while the pure precursors, before any heat treatment, are shown in Fig. S1.

Nitrogen adsorption–desorption experiments isotherms (Fig. S3) for nitrogen-containing HC show that the amount of adsorbed gas is very low (BET specific surface areas are lower than 10 m^2/g), and no specific porosity is actually detected. Isotherms show the typical behaviour of interparticle adsorption, suggesting that the microstructure of the material is formed of aggregated particles, in complete agreement with TEM analysis. Lack of developed porosity is generally associated with these materials [39] some exceptions exist for few specific cases, in which a more developed porosity can be achieved in the absence of an external porogen by forming monoliths from starch [24] or by reducing to the nanoscale the size of the aggregated particles [40]. Upon further carbonization some more micropores are developing, and there is a slight increase in the surface areas up to ~30–50 m^2/g in all materials due to an increase in microporosity.

Some interesting results come from the elemental analysis of pure and carbonized samples (Table 1). It is found that, after hydrothermal carbonization, the chitosan-derived (HC-CH) material has a carbon content of 59 wt%, lower than the one obtained for HC-GA and HC-G (about 65 wt%). Glucosamine and glucose-derived carbons contain instead about 65 wt% C (Table 1). The amount of nitrogen is as high as 9 wt% in HC-CH sample and ~6.8 wt% in HC-GA sample. Upon hydrothermal carbonization the carbon content for all the samples obviously increases, which is mainly due to the loss of oxygen and hydrogen in the dehydration process of the saccharides, while the amount of nitrogen is actually

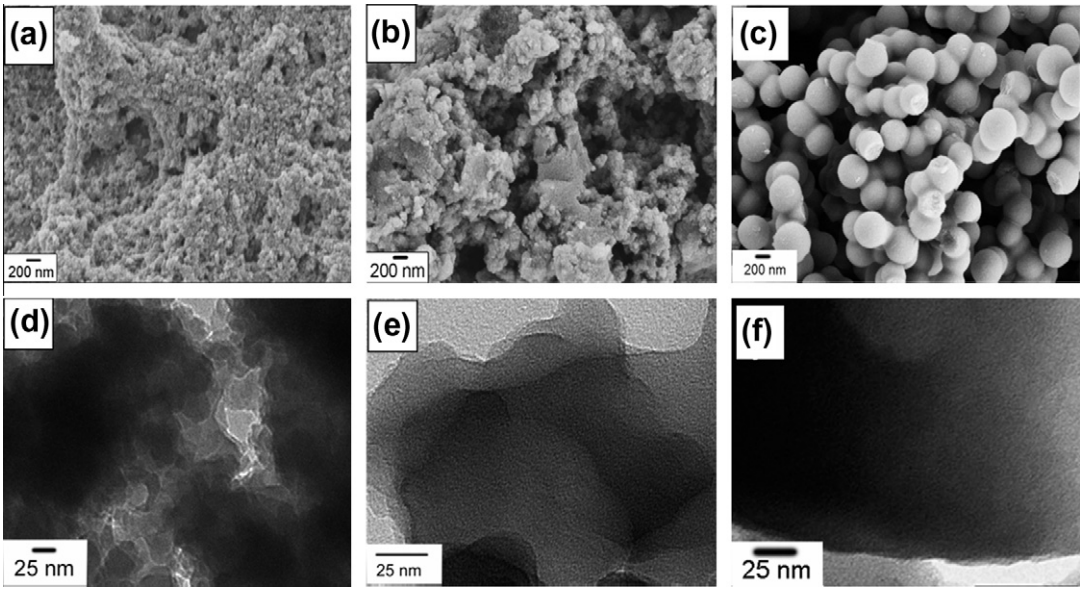

Fig. 1 – Scanning (a)–(c) and transmission (d)–(f) electron micrographs of the nitrogen-doped carbons obtained upon hydrothermal carbonization of (a) and (d) chitosan (HC-CH); (b) and (e) glucosamine (HC-GA) (c) and (f) glucose (HC-G).

Table 1 – Weight and atomic percentages of the carbon-based materials as obtained by elemental analysis and XPS respectively.

Material	From chemical analysis			From XPS		
	%C	%N	C/N	%C	%N	C/N
Pure-G	40.0	–	–		–	–
Pure-CH	32.8	9.4	3.5	65.7	9	7.3
Pure-GA	33.4	6.5	5.1	74.1	8.5	8.7
HC-G	66.6	–	–		–	–
HC-G-750	89.6	–	–		–	–
HC-CH	56.2	8.9	6.3	72.5	5.2	13.9
HC-CH-750	79.2	9.1	8.8	87.7	7.7	11.4
HC-GA	66.6	6.7	9.9	79.9	5.6	14.3
HC-GA-750	81.6	6.6	12.4	90.5	6.3	14.4

maintained constant, thus evidencing that no specific mechanism leading to the elimination of nitrogen takes place. This is interesting as it implies that nitrogen is stored in stable bonds; volatile aminated compounds, if produced, react further with the carbonaceous scaffold, as previously reported [41–43]. After further high temperature carbonization, the carbon content increases up to 89%, as expected, while the nitrogen content stays virtually constant (Table 1). This suggests that indeed nitrogen is incorporated within the carbon matrix upon hydrothermal carbonization and that, upon further heat treatment, it can actually be incorporated in the aromatization/pseudo-graphitization process of the carbon structure.

3.2. *Bulk analysis*

Solid state NMR revealed to be a powerful technique to study the structure of hydrothermal carbons, which was mainly resolved as a 3D cross-linked network of furan rings. Here, ^{13}C and ^{15}N NMR are used to characterize the structure of amino-derived carbons both after hydrothermally treatment and after further calcination at 750 °C. Unfortunately, the low natural isotopic abundance of ^{15}N (0.32%) and the lack of a (affordable) ^{15}N source prevents us from performing ^{15}N NMR experiments with good signal-to-noise ratios. ^{15}N CP-MAS experiments at natural abundance did not provide any signal in a reasonable amount of time (60 h), and for this reason, we were forced to apply weak isotopic enrichment using 1 wt% of N15-labeled glucosamine. One-pulse experiments are much more time-consuming but have the advantage of providing a full insight of all nitrogen species while CP experiments are time-saving but only provide information on nitrogen atoms with a nearby protonated environment. According to both one pulse and CP experiments, two distinct nitrogen families of comparable amount exist in the HC-GA sample. The main peak at −243 ppm (Fig. 2) indicates the existence of protonated C-NH-C groups, either in the pyrrole-like or amide forms [44,45]. Interestingly, the presence of free amino groups (−300 ppm < δ < −400 ppm) derived from glucosamine seems to be highly reduced or even disappeared, as suggested by the arguable low intensity peak at −350 ppm. Given the low signal-to-noise ratio, one-pulse experiments do not provide any quantitative answer; nevertheless, one can safely state that primary amines have massively reacted. Fig. 2 shows two one-pulse experiments which have been acquired at

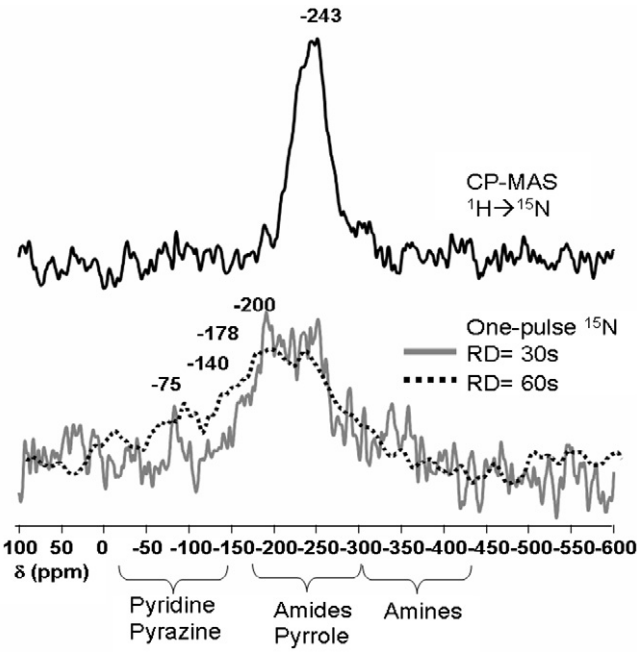

Fig. 2 – ^{15}N CP-MAS and one-pulse experiments performed on the HC-GA sample. N15 enrichment was necessary. RD = recycle delay.

two different values of recycling delay, RD = 30 s and 60 s. With respect to CP-MAS, the one-pulse experiment at RD = 30 s (solid grey line) shows the presence of a signal in the 200 ppm region, whose intensity is comparable with the signal at 243 ppm. The 200 ppm signal indicates the presence of additional de-protonated amide groups inside the carbonaceous scaffold. Moreover, the same one-pulse experiment at longer recycling delays (RD = 60 s, black dotted line) shows a broad hump between −78 and −200 ppm [44,45]; this is the fingerprint of conjugated, pyridine-like, C–N = C aromatic networks. Due to the probably very long spin-network relaxation times of nitrogen in all these chemical species, longer RD should be used to recover their full signal; which was however result in extremely long, difficult to realize, N15 experiments.

Several literature reports exist on the degradation mechanisms of GA in water at high temperatures [41–43], and in most cases, they agree on the fact that glucosamine dehydrates into

hydroxymethyl furfural (HMF), which is also the major transformation product of glucose dehydration under the same conditions [46,47], and release of ammonia in solution. Then, NH_3 readily reacts with HMF to form several type of N-containing molecules [42,43]. In general, pyrrole-like [42] or pyridine and pyrazine [42,43] compounds are described but the possibility to form amide bonds exist [41]. Interestingly, in many cases, the furanic moiety is kept throughout the process, and it is substituted by nitrogen at different positions. The ^{15}N experiments presented above on the HC-GA sample indicate a large amount of protonated, substituted pyrrole-like molecules or amide bonds. Aromatic C–N = C compounds, even if their identification is a difficult task, are also formed. We believe that several mechanisms may take place to transform glucosamine into N-carbon. The preferred mechanism of formation of HC-GA should pass through the production of ammonia and its reaction with HMF or similar furanic compounds. Considered the lower amount of aromatic amines, the mechanism leading to aromatic amines (e.g., dimerization of two glucosamine moieties, as proposed by Jun et al. [43]) does not abundantly take place here. ^{13}C NMR data shown below suggest a strong aromaticity for HC-GA with respect to HC-G, supporting the idea that aromatic amines are distributed throughout the material.

^{13}C CP MAS NMR was performed on all amino-derived samples and the results are as shown in Fig. 3. As a matter of comparison, we report the typical spectrum of a pure hydrothermal carbon from glucose (HC-G) in Fig. 3B. A crude attribution can be done as follows: δ = 10–50 ppm: aliphatic CH_x groups; δ = 100–150: aromatic range, mainly dominated by the furanic ring (sp^2 β-carbons resonate between 100 and 130 ppm while oxygenated α-carbons resonate between 130 and 150 ppm). Only less than 6% of total carbons are involved in a pure graphite-like structure (peak at 130 ppm). Peaks at 175 and 210 ppm belong to the different carbonyl groups. When thermal treatment at 750 °C is applied, the corresponding spectrum (A) shows a single main peak between 125 and 130 ppm, with a clear loss of all aliphatic and carbonyl groups and the furanic doublet. This behaviour is rather typical for a strong aromatization/pseudo-graphitization of the material.

Some changes in the ^{13}C CP MAS behaviour are found when using gluosamine as the direct nitrogen-containing source for HC (HC-GA, Fig. 3D). If aliphatic and carbonyl regions do not show major changes, the amount of COOH groups at 175 ppm seem to have relatively decreased or, at least, the peak seem to be broader. This behaviour is indicative for the reaction of the carboxylic species. The aromatic region (100–150 ppm), on the contrary, shows a single, main contribution between 125 and 130 ppm, suggesting occurrence of the aromatization/pseudo-graphitization already throughout the hydrothermal treatment. Secondary peaks due to furanes at 150 and 110 ppm can also be identified. These data show that the structure of the GA-derived carbons is far from being similar to the one of the glucose-derived hydrothermal carbons, with HC-GA having strong N-heterocyclic aromaticity while having only a weak contribution from furanic moieties.

Calcination at 750 °C (sample HC-GA-750) provides the general effect found for all hydrothermal carbons: loss of all aliphatic and carbonyl peaks while intensification of the peak

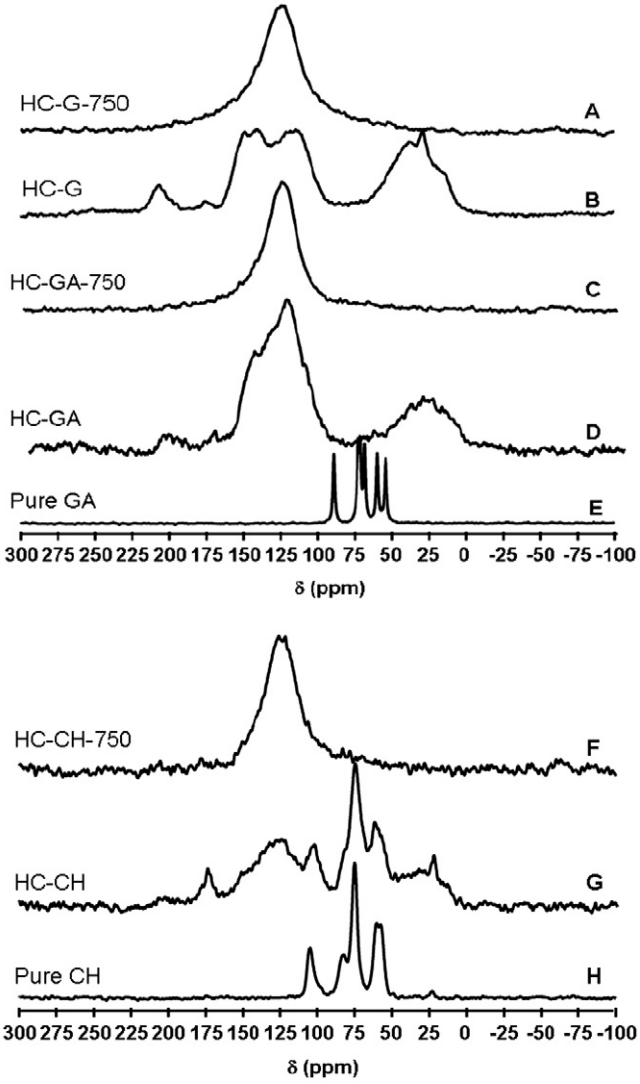

Fig. 3 – ^{13}C CP-MAS experiments performed on the pure precursors, the hydrothermally treated and carbonized (750 °C) samples.

between 125 and 130 ppm suggests a wide aromatization/pseudo-graphitization of the carbon samples. Residual presence of a shoulder peak in the 150 ppm area is still sign of oxygenated and/or aminated sp^2 carbons. When comparing the ^{13}C NMR spectra of the glucosamine-based HC-GA materials (Fig. 3 spectrum D) with a pure glucosamine sample (Fig. 3 spectra E), it is quite evident that almost the whole amount of the amino-sugar has reacted, as its peaks between 50 and 75 ppm have disappeared. On the contrary, the chitosan-derived HC materials (Fig. 5, spectrum G) still possesses strong signals. This might be due to the fact that chitosan is a linear polysaccharide composed of randomly distributed β-(1-4)-linked D-glucosamine units and therefore would require higher temperatures that 180 °C to be fully converted into HTC since it needs firs to be broken into its individual monomers. Furthermore, the glucosamine used in this experiment was in its hydrochloride form which then might decrease the pH of the solution acting thus as a catalyst for the hydrothermal carbonization of glucosamine.

Therefore, the ^{13}C solid state CP MAS NMR analysis shows that the hydrothermal treatment of aminated sugars enhances the carbonization process towards more aromatic carbons with extended graphitic domains already throughout hydrothermal treatment at 180 °C, while the differently aminated chitosan results in lower carbonization efficiencies along the traditional reaction scheme. These data also nicely mirror the elemental analysis results.

3.3. *Surface analysis*

Surface properties of the carbonaceous materials were characterized with XPS and ζ-potential measurements. XPS analysis was performed on the pure starting precursors, on the hydrothermally treated samples and on the carbonized samples. Detailed spectra were collected for the three regions of interest (N1s reported in Fig. 4, C1s reported in Fig. S4, and O1s (not shown)) from which the atomic percentages of the three elements were determined. Those of C and N are reported in Table 1. As it can be evidenced by comparing the atomic percentage values obtained by XPS with those calculated from the weight percentages delivered by elemental analysis, the amounts of carbon detected by XPS is systematically higher that the atomic percentages calculated starting from the experimental weight percentages obtained by elemental analysis.

Remarkably, atomic percentage values for nitrogen are high for all samples and, in agreement with elemental analysis, their values increase with increasing thermal treatment.

The XPS spectra for the chitosan series are shown together with a deconvolution of the C1s and N1s peaks in Fig. S4 and Fig. 4, respectively. The values for the binding energies

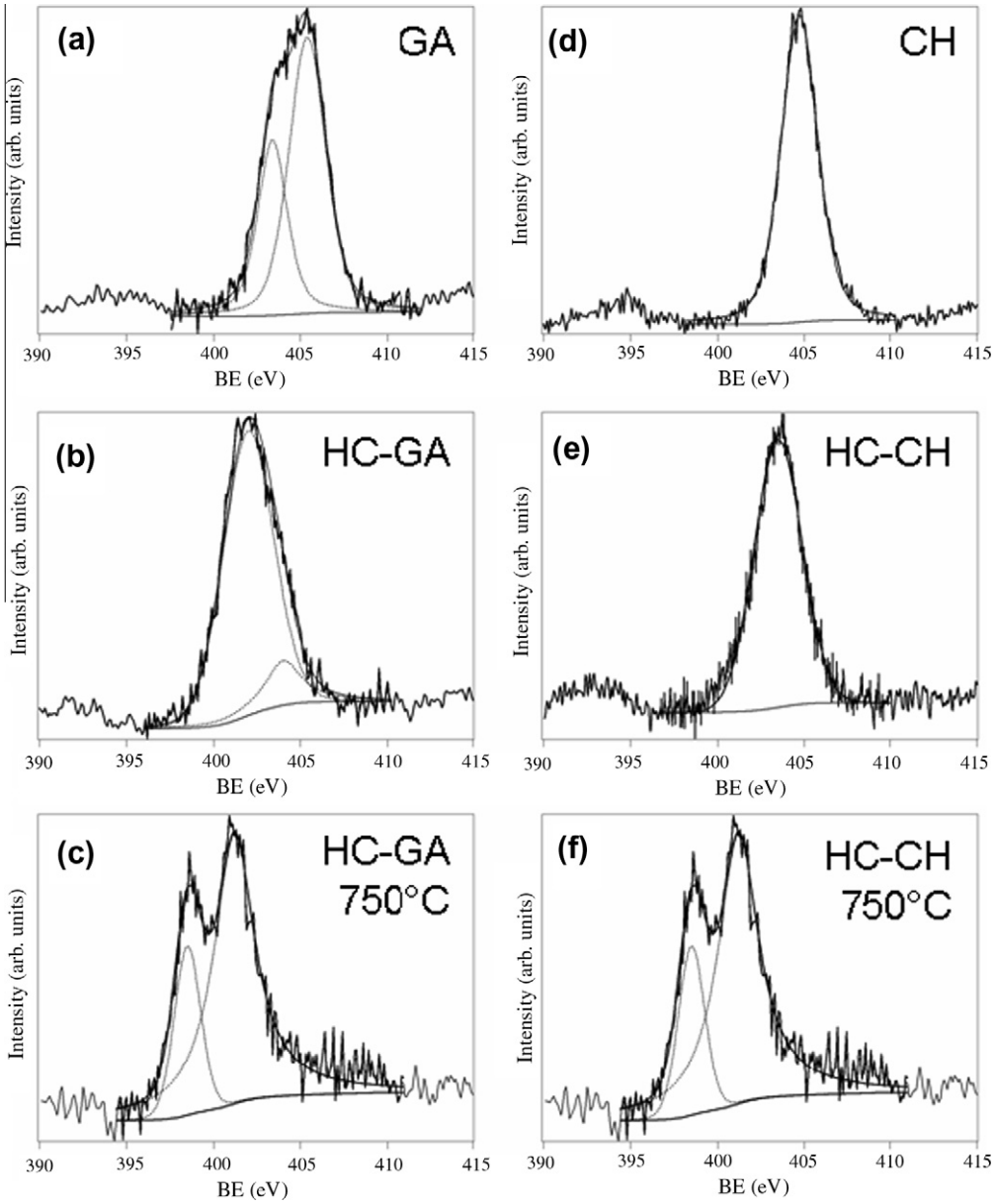

Fig. 4 – N1s signals of the pure, hydrothermally treated and calcined glucosamine (GA) and chitosan (CH) samples. The values in the abscissa are not corrected for charging effects. Refer to discussion in the text or to Table 1 for corrected values.

together with their assessments are presented in Table S1 in the supplementary material. In the case of pure chitosan, according to references reported in the literature [48], three different carbon components could be identified: the more intense one, at 286.1 eV, was ascribed to carbon bonded to –OH and/or OR groups, whereas the component at lower BE (284.6 eV) was assigned to aliphatic carbon/adventitious carbon; the one at higher BE (287.9 eV) is attributed to C–O–C moieties. After the hydrothermal carbonization, the band at 284.6 eV corresponding to the C–H/C–C bonds (sp^3 hybridized carbon) is still present meaning in this sample, as previously shown by ^{13}C-solid state NMR experiments (see Fig. 3). However some changes as compared to the pure chitosan occur. Parts of the oxygenated functionalities are maintained in the hydrothermal carbon material as normally in hydrothermal carbonization [49]. However, after further carbonization at higher temperatures major changes in the structure are visible. First of all, a decrease in oxygen content and an increase in the C/N ratio is observed. Secondly the sample derived from chitosan treated at 750 °C present a major C1s component at 285.1 eV, ascribed to a graphitic-like structure, a weak component at 289.5 eV corresponding π–π^* shake up, indicative of extended aromatic features, and another weak components at 286.9, ascribed to oxygenated moieties, which is remarkably less intense than in the not treated samples, evidencing that almost all the oxygenated functionalities were removed from the sample, in agreement with quantitative analysis showing a drop of oxygen atomic (from 22.3% to 4.7%) and ^{13}C solid state NMR. The same trend could be observed also in the glucosamine-derived sample. This component at 285.1 eV corresponds to a predominantly sp^2 hybridized aromatic (reference value 284.8–285.1 eV).

Concerning the N1s peak (Fig. 4), the pure chitosan sample shows only one component which according to the binding energy value (399.3 eV) corresponds to the primary amine group, as expected. After hydrothermal carbonization the binding energy shifts from 399.3 to 402.1 eV, thus suggesting that the amino group has undergone a chemical reaction leading to the formation of quaternary N (reference values: 400.8–402.0 eV) [16,50,51]. Upon even further heat treatment at higher temperature (750 °C), the N1s region could be fitted with two components, with very different positions with respect to the untreated samples: at 401.2 and a less intense at 398.5 eV, with an intensity ratio of about 3:1. Whereas the former component was ascribed to N in aromatic graphene structure [16,50], the second one has a value which is typical of that reported for pyridinic (aromatic) nitrogen (reported values: 398.1–399.0 eV) [51].

A similar trend can be observed in the case of glucosamine precursor. Thus, the C1s spectra of the pure precursors show the presence of two components of C-H/C-C, of C-OH and C-O-C bonds, which are also maintained after the hydrothermal carbonization. Clear differences between the pure precursors and the hydrothermal carbonized materials do not appear to be significant in XPS. This shows that in the case of glucosamine-derived carbons, the surface of the material is aliphatic-rich. From ^{13}C solid state NMR (Fig. 3), we know that glucosamine has gone under full reaction after hydrothermal treatment; this means that the carbon species detected by XPS do not belong to the glucosamine molecule but rather to C-H and C-O-C groups derived from the carbonization process and largely described in [52].

Further heat treatment of the HC-GA product, again a very discreet C 1s spectrum with bands was observed at 285.1 eV corresponding to an aromatic system, and much less intenses at 287.1 eV and 290.0 eV corresponding to C-OH moieties and π–π^* shake up.

As far as pure glucosamine is concerned, the N1s region contains two components, at 398.5 and 400.5 eV, corresponding to amine and to protonated amine groups (the starting product is an acidified glucosamine). In the case of HC-GA, the N1s peak shows two components at 399.3 and 401.3 eV, respectively. The former can be ascribed to pyridinic nitrogen, the latter to N in condensed polyaromatic structure, in agreement with what observed by NMR. Upon further carbonization at 750 °C, two components at 398.5 eV and 401.2 eV, ascribed to pyridinic N [53] and to N in aromatic graphene structure, respectively, could be observed. XPS data confirm ^{15}N NMR experiments (Fig. 2) showing that nitrogen is incorporated into the core of a more aromatized system.

The structural study performed so far by XPS and NMR suggests an altered growth under hydrothermal treatment of amino-group containing carbohydrates. We have shown that the mechanism of transformation of glucose into carbon-like materials under hydrothermal conditions involves the dehydration of glucose to hydroxymethylfurfural (HMF) in the first step, followed by the polymerization and aromatization of the latter to produce the carbonaceous material [21,54]. In the case of amino containing carbohydrates, the transformation process is much more complex, as we previously discussed. In addition, Maillard-type reactions (very well known in food chemistry [53,55] between HMF (containing an aldehyde group) and the amine may also take place and lead towards nitrogen-containing heterocycles. This scenario is also supported by the GC–MS spectra of the liquid phase obtained upon hydrothermal carbonization of chitosan and glucosamine (data not shown), which shows only small traces of HMF in comparison with pure glucose, but shows indeed nitrogen-containing heterocycles which are not detected in the case of pure glucose. In addition, consumption of amine groups is also clear from CP-MAS ^{15}N solid state NMR spectra of HC-GA (Fig. 3).

Zeta-potential experiments as a function of pH on aqueous dispersions of the samples (Fig. 5) can help to further characterize the nitrogen functions. The as-synthesized HC-CH and HC-GA hydrothermal powders (Fig. 5a) clearly show positive zeta-potentials below pH $\sim$ 5 and 6, indicating the existence of positively charged, accessible amino groups at the particle's surface with values up to 30 mV at pH 2.5. These data are coherent with XPS analysis, which have showed that roughly 6% of nitrogen sites at the material surface, and ^{15}N NMR data. On the contrary, pure hydrothermal carbon (HC) from glucose shows no positive zeta-potential value in the whole examined range, as previously described [40]. Analyzing the effects of calcination on the zeta-potential (Fig. 5b), it is found that the positive character is clearly diminished by the temperature treatment. A nearby explanation in agreement with XPS data evidencing the nitrogenated functions is that the nitrogen is now incorporated into the aromatic carbon system and therefore has a much less basic in character.

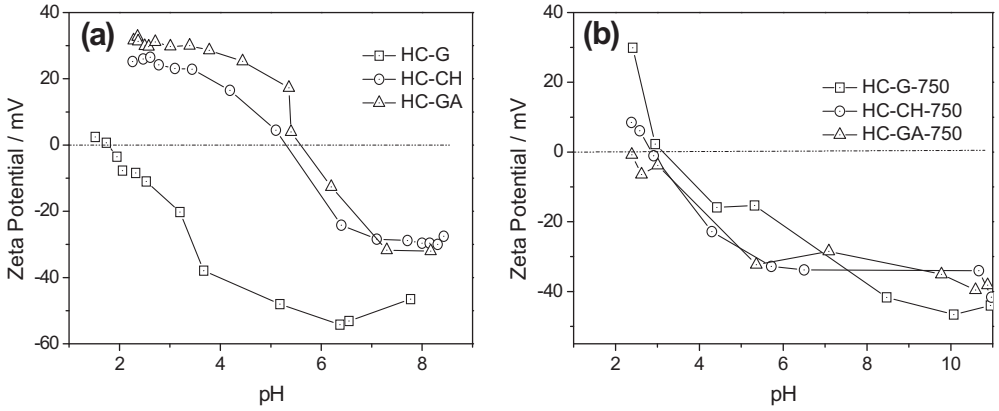

Fig. 5 – Zeta-potential experiments of (a) HC-G, HC-CH and HC-GA; (b) HC-G-750, HC-CH-750 and HC-GA-750.

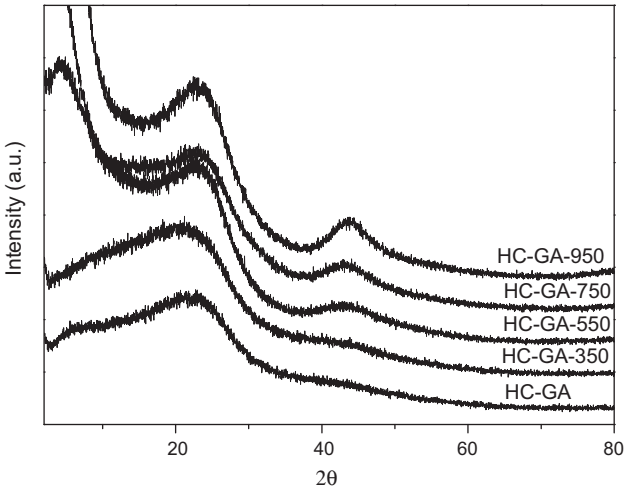

Fig. 6 – XRD profiles of the carbons obtained from glucosamine at different temperatures.

Table 2 – Conductivities of HC-G-750, HC-CH-750 and HC-GA-750.

Sample	HC-G-750	HC-CH-750	HC-GA-750
Conductivity (S/m)	80.3 ± 10.5	100.3 ± 19.5	103.7 ± 9.7

3.4. *Structural order and electronic conductivity*

XRD measurements on the prepared samples show one single broad reflection around 25° 2 theta corresponding to the (0 0 2) interlayer reflection for the HC-GA and HC-GA-350. A second peak at about 45° 2 theta characteristic for the (1 0 0) in-plane scattering starts appearing for the samples treated at 550 °C and above. This demonstrates that at low temperatures, the sample has an amorphous structure whose order improves towards a turbostatic type of carbon with increasing the temperature (Fig. 6).

As stated above, nitrogen-doped carbons are interesting materials due to their improved performance. Like other carbon nanostructures such as carbon nanotubes, hydrothermal carbon's electronic band structure was also probably significant influenced by nitrogen doping [52]. Therefore, conductivity measurements of samples after further carbonization at 750 °C were undertaken. Results shown in Table 2 that nitrogen doped hydrothermal carbon based on chitosan and glucosamine, show an improved electronic conductivity with respect to the glucose based carbon.

4. Conclusion

We have demonstrated that it is possible to synthesize nitrogen containing carbonaceous materials by hydrothermal treatment of amino containing carbohydrates at 180 °C. Besides being green, cheap and sustainable, this process has the advantage to introduce nitrogen dopants into the carbonaceous scaffold, which are known to be very favorable for catalysis, adsorption, or energy storage devices Various characterization methods (nitrogen adsorption-desorption, TEM, SEM, XPS, ^{13}C-solid state NMR, XRD, zeta potential and elemental analysis) were used to describe the resulting carbon structures. Temperature treatments showed that all materials retain the nitrogen content almost unchanged up to 750 °C. Maybe one of the most important benefits of the nitrogen containing monomers is the fact that we can generate spontaneous aromatization already at 180 °C in a hydrothermal treatment, appropriate ammonia releasing monomers assumed. Last but not least, the whole synthetic process occurs in an energy and atom-saving fashion from cheap and sustainable resources, as employed temperatures in the first step remain below 200 °C, and neither metals nor surfactants have been used to catalyze and control the reaction.

The beneficial properties were exemplified by the conductivity measurements where an increase of the direct current conductivity was found for the nitrogen containing materials. We are presently also investigating the performance of such nitrogen containing carbon materials in fields such CO_2 sequestration, supercapacitors as well as catalysts. The preliminary results are very promising, especially in the field of selective CO_2 sequestration, showing such easy produced materials could be of major importance.

Appendix A. Supplementary material

Supplementary data associated with this article can be found, in the online version, at doi:10.1016/j.carbon.2010.06.040.

REFERENCES

[1] Mauter MS, Elimelech M. Environmental applications of carbon-based nanomaterials. Environ Sci Technol 2008;42(16):5843–59.

[2] Huang CP, Wu MH. Removal of chromium(Vi) from dilute aqueous-solution by activated carbon. Water Res 1977;11(8):673–9.

[3] Pantarotto D, Briand JP, Prato M, Bianco A. Translocation of bioactive peptides across cell membranes by carbon nanotubes. Chem Commun 2004;7(1):16–7.

[4] Yan AH, Lau BW, Weissman BS, Kulaots I, Yang NYC, Kane AB, et al. Biocompatible, hydrophilic, supramolecular carbon nanoparticles for cell delivery. Adv Mater 2006;18(18):2373–8.

[5] Dillon AC, Jones KM, Bekkedahl TA, Kiang CH, Bethune DS, Heben MJ. Storage of hydrogen in single-walled carbon nanotubes. Nature 1997;386(6623):377–9.

[6] Zakhidov AA, Baughman RH, Iqbal Z, Cui CX, Khayrullin I, Dantas SO, et al. Carbon structures with three-dimensional periodicity at optical wavelengths. Science 1998;282(5390):897–901.

[7] Hsieh CT, Teng H. Influence of oxygen treatment on electric double-layer capacitance of activated carbon fabrics. Carbon 2002;40(5):667–74.

[8] Hulicova D, Kodama M, Hatori H. Electrochemical performance of nitrogen-enriched carbons in aqueous and non-aqueous supercapacitors. Chem Mater 2006;18(9):2318–26.

[9] Lin Y, Rao AM, Sadanadan B, Kenik EA, Sun YP. Functionalizing multiple-walled carbon nanotubes with aminopolymers. J Phys Chem B 2002;106(6):1294–8.

[10] Plaza MG, Pevida C, Arenillas A, Rubiera F, Pis JJ. CO_2 capture by adsorption with nitrogen enriched carbons. Fuel 2007;86(14):2204–12.

[11] Stavropoulos GG, Samaras P, Sakellaropoulos GP. Effect of activated carbons modification on porosity, surface structure and phenol adsorption. J Hazard Mater 2008;151(2–3):414–21.

[12] Jia YF, Xiao B, Thomas KM. Adsorption of metal ions on nitrogen surface functional groups in activated carbons. Langmuir 2002;18(2):470–8.

[13] Shao YY, Sui JH, Yin GP, Gao YZ. Nitrogen-doped carbon nanostructures and their composites as catalytic materials for proton exchange membrane fuel cell. Appl Catal B 2008;79(1–2):89–99.

[14] Weydanz WJ, Way BM, van Buuren T, Dahn JR. Behavior of nitrogen-substituted carbon (NzC_1-z) in Li/Li(NzC_1-z)$_6$ cells. J Electrochem Soc 1994;141(4):900–7.

[15] Nxumalo EN, Nyamori VO, Coville NJ. CVD synthesis of nitrogen doped carbon nanotubes using ferrocene/aniline mixtures. J Organomet Chem 2008;693(17):2942–8.

[16] Burg P, Fydrych P, Cagniant D, Nanse G, Bimer J, Jankowska A. The characterization of nitrogen-enriched activated carbons by IR, XPS and LSER methods. Carbon 2002;40(9):1521–31.

[17] Huang MC, Teng HS. Nitrogen-containing carbons from phenol-formaldehyde resins and their catalytic activity in NO reduction with NH_3. Carbon 2003;41(5):951–7.

[18] Yang Z, Xia Y, Sun X, Mokaya R. Preparation and hydrogen storage properties of zeolite-templated carbon materials nanocast via chemical vapor deposition: effect of the zeolite template and nitrogen doping. J Phys Chem B 2006;110(37):18424–31.

[19] Hou PX, Orikasa H, Yamazaki T, Matsuoka K, Tomita A, Setoyama N, et al. Synthesis of nitrogen-containing microporous carbon with a highly ordered structure and effect of nitrogen doping on H_2O adsorption. Chem Mater 2005;17(20):5187–93.

[20] Budarin V, Clark JH, Hardy JJE, Luque R, Milkowski K, Tavener SJ, et al. Starbons: new starch-derived mesoporous carbonaceous materials with tunable properties. Angew Chem Int Ed 2006;45(23):3782–6.

[21] Titirici MM, Antonietti M, Baccile N. Hydrothermal carbon from biomass: a comparison of the local structure from poly- to monosaccharides and pentoses/hexoses. Green Chem 2008;10(11):1204–12.

[22] Titirici MM, Thomas A, Yu SH, Muller JO, Antonietti M. A direct synthesis of mesoporous carbons with bicontinuous pore morphology from crude plant material by hydrothermal carbonization. Chem Mater 2007;19(17):4205–12.

[23] Wang Q, Li H, Chen LQ, Huang XJ. Monodispersed hard carbon spherules with uniform nanopores. Carbon 2001;39(14):2211–4.

[24] Budarin V, Luque R, Macquarrie DJ, Clark JH. Towards a bio-based industry: benign catalytic esterifications of succinic acid in the presence of water. Chem Eur J 2007;13(24):6914–9.

[25] Sun XM, Li YD. Colloidal carbon spheres and their core/shell structures with noble-metal nanoparticles. Angew Chem Int Ed 2004;43(5):597–601.

[26] Titirici MM, Antonietti M, Thomas A. A generalized synthesis of metal oxide hollow spheres using a hydrothermal approach. Chem Mater 2006;18(16):3808–12.

[27] Yu SH, Cui XJ, Li LL, Li K, Yu B, Antonietti M, et al. From starch to metal/carbon hybrid nanostructures: hydrothermal metal-catalyzed carbonization. Adv Mater 2004;16(18):1636–40.

[28] Zhu K, Egeblad K, Christensen CH. Mesoporous carbon prepared from carbohydrate as hard template for hierarchical zeolites. Eur J Inorg Chem 2007(25):3955–60.

[29] Berl E, Schmidt A, Koch H. The development of carbon. Angew Chem 1932;45:0517–9.

[30] Corma A, Iborra S, Velty A. Chemical routes for the transformation of biomass into chemicals. Chem Rev 2007;107(6):2411–502.

[31] Titirici MM, Thomas A, Antonietti M. Back in the black: hydrothermal carbonization of plant material as an efficient chemical process to treat the CO_2 problem? New J Chem 2007;31(6):787–9.

[32] Seah MP. Practical Surface Analysis. In: Briggs D, Seah MP, editors. J. Wiley & Sons; 1990. p. 543.

[33] Moulder JF, Stickle WF, Sobol PE, Bomben KD. Handbook of X-ray photoelectron spectroscopy. In: Chastain J, editor. Perkin–Elemer Corp., Eden Prairie, MN; 1992.

[34] Shirley DA. High-resolution X-ray photoemission spectrum of valence ands of gold. Phys Rev B 1972;5(12):4709–14.

[35] X-ray photoelectron spectroscopy database 20, Version 3.0, National Institute of Standards and Technology, Gaithersburg, MD [cited; Available from: http://srdata.nist.gov/XPS].

[36] Makowski P, Cakan RD, Antonietti M, Goettmann F, Titirici MM. Selective partial hydrogenation of hydroxy aromatic derivatives with palladium nanoparticles supported on hydrophilic carbon. Chem Commun 2008(8):999–1001.

[37] Hu YS, Demir-Cakan R, Titirici MM, Muller JO, Schlogl R, Antonietti M, et al. Superior storage performance of a Si@SiOx/C nanocomposite as anode material for lithium-ion batteries. Angew Chem Int Ed 2008;47(9):1645–9.

[38] Demir-Cakan R, Baccile N, Antonietti M, Titirici MM. Carboxylate-rich carbonaceous materials via one-step

hydrothermal carbonization of glucose in the presence of acrylic acid. Chem Mater 2009;21(3):484–90.
[39] Titirici MM, Antonietti M. Chemistry and materials options of sustainable carbon materials made by hydrothermal carbonization. Chem Soc Rev 2010;39(1):103–16.
[40] Baccile N, Antonietti M, Titirici MM. One-step hydrothermal synthesis of nitrogen-doped nanocarbons: albumine directing the carbonization of glucose. ChemSusChem 2009 [doi: 10.1001/cssc.200900124].
[41] Chen J, Wang M, Ho C-T. Volatile compounds generated from thermal degradation of N-acetylglucosamine. J Agric Food Chem 1998;46(8):3207–9.
[42] Shu C-K. Degradation products formed from glucosamine in water. J Agric Food Chem 1998;46(3):1129–31.
[43] Jun M, Shao YY, Ho C-T, Koetter U, Lech S. Structural identification of nonvolatile dimerization products of glucosamine by gas chromatography–mass spectrometry, liquid chromatography–mass spectrometry, and nuclear magnetic resonance analysis. J Agric Food Chem 2003;51(21):6340–6.
[44] Levy GC, Lichter RL, Nitrogen-15 nuclear magnetic resonance spectroscopy. New Your: Wiley; 1979.
[45] Gammon WJ, Hoatson GL, Holloway BC, Vold RL, Reilly AC. Bonding in hard and elastic amorphous carbon nitride films investigated using N-15, C-13, and H-1 NMR spectroscopy. Phys Rev B 2003;68(19):195401-1-8.
[46] Asghari FS, Yoshida H. Acid-catalyzed production of 5-hydroxymethyl furfural from d-fructose in subcritical water. Ind Eng Chem Res 2006;45(7):2163–73.
[47] Ulbricht RJ, Northup SJ, Thomas JA. A review of 5-hydroxymethylfurfural (HMF) in parenteral solutions. Fundam Appl Toxicol 1984;4(5):843–53.
[48] Liu Y, Gaskell KJ, Cheng ZH, Yu LL, Payne GF. Chitosan-coated electrodes for bimodal sensing: selective post-electrode film reaction for spectroelectrochemical analysis. Langmuir 2008;24(14):7223–31.
[49] Sevilla M, Fuertes AB. Chemical and structural properties of carbonaceous products obtained by hydrothermal carbonization of saccharides. Chem Eur J 2009;15(16):4195–203.
[50] Lahaye J, Nanse G, Bagreev A, Strelko V. Porous structure and surface chemistry of nitrogen containing carbons from polymers. Carbon 1999;37(4):585–90.
[51] Pietrzak R, Wachowska H, Nowicki P. Preparation of nitrogen-enriched activated carbons from brown coal. Energy Fuels 2006;20(3):1275–80.
[52] Baccile N, Laurent G, Babonneau F, Fayon F, Titirici MM, Antonietti M. Structural characterization of hydrothermal carbon spheres by advanced solid-state MAS C-13 NMR investigations. J Phys Chem C 2009;113(22):9644–54.
[53] Bravo A, Herrera JC, Scherer E, Ju-Nam Y, Rubsam H, Madrid J, et al. Formation of alpha-dicarbonyl compounds in beer during storage of Pilsner. J Agric Food Chem 2008;56(11):4134–44.
[54] Lourvanij K, Rorrer GL. Dehydration of glucose to organic-acids in microporous pillared clay catalysts. Appl Catal A 1994;109(1):147–65.
[55] Harrison TJ, Dake GR. Expeditious, high-yielding construction of the food aroma compounds 6-acetyl-1, 2, 3, 4-tetrahydropyridine and 2-acetyl-1-pyrroline. J Org Chem 2005;70(26):10872–4.